Fundamental Research 4 (2024) 57–62

Contents lists available at ScienceDirect

Fundamental Research

journal homepage: http://www.keaipublishing.com/en/journals/fundamental-research/

Article

Acoustic Purcell effect induced by quasibound state in the continuum

Sibo Huang[a,b,1], Shuhuan Xie[a,c,1], He Gao[b], Tong Hao[c], Shuang Zhang[d], Tuo Liu[e,*], Yong Li[a,*], Jie Zhu[a,b,f,*]

[a] Institute of Acoustics, School of Physics Science and Engineering, Tongji University, Shanghai 200092, China
[b] Department of Mechanical Engineering, The Hong Kong Polytechnic University, Hong Kong 999077, China
[c] College of Surveying and Geo-Informatics, Tongji University, Shanghai 200092, China
[d] Department of Physics, The University of Hong Kong, Hong Kong 999077, China
[e] Key Laboratory of Noise and Vibration Research, Institute of Acoustics, Chinese Academy of Sciences, Beijing 100190, China
[f] The Hong Kong Polytechnic University Shenzhen Research Institute, Shenzhen 518057, China

ARTICLE INFO

Article history:
Received 31 March 2022
Received in revised form 18 May 2022
Accepted 20 June 2022
Available online 30 June 2022

Keywords:
Acoustic Purcell effect
Bound state in the continuum
Mode coupling
Sound emission enhancement
High-quality-factor acoustic device

ABSTRACT

We study theoretically and experimentally the acoustic Purcell effect induced by quasi-bound states in the continuum (quasiBICs). A theoretical framework describing the acoustic Purcell effect of a resonant system is developed based on the system's radiative and dissipative factors, which reveals the critical emission condition for achieving optimum Purcell factors. We show that the quasiBICs contribute to highly confined acoustic field and bring about greatly enhanced acoustic emission, leading to strong Purcell effect. Our concept is demonstrated via two coupled resonators supporting a Friedrich–Wintgen quasiBIC, and the theoretical results are validated by the experiments observing emission enhancement of the sound source by nearly two orders of magnitude. Our work bridges the gap between the acoustic Purcell effect and acoustic BICs essential for enhanced wave-matter interaction and acoustic emission, which may contribute to the research of high-intensity sound sources, high-quality-factor acoustic devices and nonlinear acoustics.

1. Introduction

The Purcell effect predicts that spontaneous radiation is not an intrinsic property of matter, but is determined by the interaction of matter with its surrounding environment [1–6]. Although this notion was first explored in quantum systems [7–9], it fundamentally reveals that the emission of sources can be modulated actively by engineering the surrounding environments, which has aroused broad interests in electromagnetic [10–15], elastic [16,17] and acoustic [18,19] wave systems. The acoustical counterpart of the Purcell effect in quantum emission has been proposed via Mie-like resonances [18] and Helmholtz resonances [19], and shown to be important for improving the low-frequency emission of loudspeakers and generating strong acoustic collimated waves [18–21]. A major challenge in achieving strong acoustic Purcell effect is that realistic acoustic systems usually suffer from non-trivial dissipative (thermal-viscous) losses and exhibit considerably low quality factors (Q), which severely restricts the highest Purcell factor one may access. More importantly, despite the importance of thermal-viscous losses, a comprehensive theoretical model that incorporates the effect of dissipative losses for describing the acoustic Purcell effect has not been developed so far.

In this study, we establish a theoretical framework with the effects of radiative and dissipative losses being considered and systematically investigate the acoustic Purcell effect. As we will show in the following, the acoustic Purcell factor is governed by the system's radiative and dissipative factors (Q_{leak}^{-1} and Q_{loss}^{-1}), and there exists a critical condition that signifies the combinations of Q_{leak}^{-1} and Q_{loss}^{-1} for the optimum Purcell factor values. To improve the upper bound of the Purcell effect, we should simultaneously decrease the values of Q_{leak}^{-1} and Q_{loss}^{-1}. However, it is rather difficult and even conflicting in realistic acoustic resonant structures (shown later). We subsequently manifest that this conflict can be well solved if we introduce the concept of quasiBIC-induced Purcell effect. Bound states in the continuum (BICs) are peculiar states perfectly confined with no radiation yet lie inside a continuous spectrum of radiating waves [22–33]. Acoustic BICs, early explored in the 1960s [34–36], exhibit infinite Q factors and feature complete isolation, which can provide high Q factors [37–41] and meanwhile allow access to external radiation when turning into quasiBICs [22,42–44], therefore providing an

* Corresponding authors.
E-mail addresses: liutuo@mail.ioa.ac.cn (T. Liu), yongli@tongji.edu.cn (Y. Li), jiezhu@tongji.edu.cn (J. Zhu).
[1] These authors contributed equally to this work.

https://doi.org/10.1016/j.fmre.2022.06.009

efficient pathway for the construction of strong Purcell effect. To demonstrate our concept, a two-state system supporting a Friedrich–Wintgen quasiBIC together with its cavity-based practical implementation is presented, offering tunable and low Q_{leak}^{-1} to approach the critical emission condition and consequently promoting the acoustic Purcell effect. The presented concept of quasiBIC-induced Purcell effect and the developed framework would open up an avenue to explore high-intensity, high-Q and nonlinear-acoustic devices.

2. Methods

2.1. Numerical simulations

All simulations in this paper are performed with the commercial finite element software COMSOL Multiphysics with the preset "Pressure Acoustics, Frequency Domain" module. In the simulations, the domain material is air (the static air density, $\rho = 1.21\ \mathrm{kg/m^3}$, the sound speed, $c = 343\ \mathrm{m/s}$, the dynamic viscosity of air, $\mu = 1.81 \times 10^{-5}\ \mathrm{N\ S/m^2}$, and the preset environmental temperature, $T = 293.15\ \mathrm{K}$ (20 °C). The detailed information of the simulations are presented in Supplementary Note 1 and Note 2.

2.2. Sample fabrications and measurements

The experimental sample is fabricated by 3D-printing technology using laser stereolithography (SLA, 140 μm) with photosensitive resin (UV curable resin) being the base material (manufacturing precision 0.1 mm). In the measurements, a loudspeaker is mounted at the bottom center of one of the cavities, and the sample is connected to a waveguide with the same cross-section. Porous sound-absorbing materials are placed at the waveguide's end to create a nonreflecting boundary. A 1/4-inch condenser microphone (Brüel & Kjær Type 4187) is situated at the designated position to test the emitted sound. The detailed experimental setup is presented in Supplementary Note 3.

3. Results and discussion

3.1. Concept of the quasiBIC-induced acoustic Purcell effect

We start by introducing the concept of the quasiBIC-induced acoustic Purcell effect (Fig. 1). For quasiBIC-supporting systems, when acoustic sources are placed inside, the emitted waves in the continuum frequency spectrum will only receive trivial or negligible influence due to the systems' normal radiation rate, while the emitted waves at the quasiBIC will be greatly enhanced thanks to the strongly confined fields within the systems [45,46]. Generally, a resonant mode of an open system can be characterized by the system's radiative and dissipative factors (Q_{leak}^{-1} and Q_{loss}^{-1}) that describe the relations of the energy stored to the energy leaked and dissipated, respectively. Thus, a theoretical framework interpreting the mode-induced acoustic Purcell effect based on Q_{leak}^{-1} and Q_{loss}^{-1} would be generic and comprehensive.

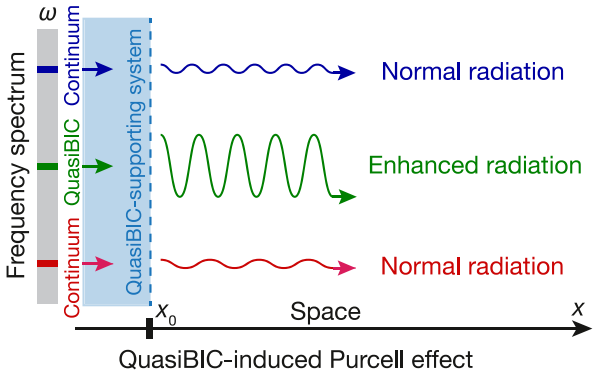

Fig. 1. Concept of the quasiBIC-induced acoustic Purcell effect. In a quasiBIC-supporting system (light-blue domain) with a sound source inside, the emitted waves at the quasiBIC (green) will be greatly confined and lead to strong enhancement. The emitted waves in the continuum frequency spectrum (grey-shaded, blue, red) will receive insignificant influence. x_0 marks the front surface of the system.

3.2. Purcell factor of an acoustic resonant system

As depicted in Fig. 2a, we consider an acoustic resonant system constructed with an effective medium. A source is placed at the bottom radiating through the interface located at x_0 to the outside. From the decomposed sound field given in the caption of Fig. 2a, Q_{leak}^{-1} and Q_{loss}^{-1} can be deduced as [47]: (see Supplementary Note 4 for details)

$$Q_{\mathrm{leak}}^{-1} = \frac{c\left|P_{\mathrm{T}}\right|^2}{\omega_0 L_{\mathrm{e}}\left(\left|P_{\mathrm{A2}}\right|^2 + \left|P_{\mathrm{B2}}\right|^2\right)} \tag{1}$$

$$Q_{\mathrm{loss}}^{-1} = \frac{c\epsilon^2\left|P_{\mathrm{A2}}\right|^2}{\omega_0 L_{\mathrm{e}}\left(\left|P_{\mathrm{A2}}\right|^2 + \left|P_{\mathrm{B2}}\right|^2\right)} \tag{2}$$

where L_{e} is the effective propagation length for waves from sound source to the system's front surface, c the sound speed, and ϵ the intrinsic-dissipation factor [48] (see Supplementary Note 4 for details).

The acoustic Purcell factor (F) can be defined as $\left|P_{\mathrm{T}}/P_{\mathrm{I}}\right|^2$, which indicates the enhancement of the source' emitted sound power to the radiation field contributed from the presented structures [16–19,45,46]. With the derivations in Supplementary Note 4, the link between the quality factors of a resonant mode and the peak acoustic Purcell factor can be obtained as:

$$F_{\mathrm{peak}} = 1 + \frac{2}{\pi Q_{\mathrm{leak}}^{-1}} + 2\sqrt{\frac{1}{\pi Q_{\mathrm{leak}}^{-1}} + \frac{1}{\left(\pi Q_{\mathrm{leak}}^{-1}\right)^2}} \tag{3}$$

$$F_{\mathrm{peak}} = \frac{Q_{\mathrm{leak}}^{-1}}{Q_{\mathrm{leak}}^{-1} + Q_{\mathrm{loss}}^{-1}} + \frac{2Q_{\mathrm{leak}}^{-1}}{\pi\left(Q_{\mathrm{leak}}^{-1} + Q_{\mathrm{loss}}^{-1}\right)^2} + 2Q_{\mathrm{leak}}^{-1}\sqrt{\frac{1}{\pi\left(Q_{\mathrm{leak}}^{-1} + Q_{\mathrm{loss}}^{-1}\right)^3} + \frac{1}{\pi^2\left(Q_{\mathrm{leak}}^{-1} + Q_{\mathrm{loss}}^{-1}\right)^4}} \tag{4}$$

where F_{peak} is the Purcell factor at the dominating mode of the system, which indicates the highest value of F in the frequency spectrum. Eqs. 3 and 4 correspond to the conditions in the absence of and in the presence of dissipative losses, respectively. Compared with the theoretical model based on the acoustic density of states (DOS) [18], the theoretical model established allows the consideration of the effect of dissipative (thermal-viscous) losses. Eq. 4 manifests that F_{peak} is determined by the mutual effect of Q_{leak}^{-1} and Q_{loss}^{-1} and reaches its optimum under the critical emission condition that reads:

$$Q_{\mathrm{leak}}^{-1} = Q_{\mathrm{loss}}^{-1}\left(1 + \pi Q_{\mathrm{loss}}^{-1}\right) \tag{5}$$

It is noteworthy that the Purcell factors described in Eqs. 3 and 4 don't contain a term of "acoustic mode volume", which is different from the commonly-used theoretical model in describing Purcell factors in quantum systems. The reason for this may be that the acoustic Purcell factor here is derived based on a simple one-dimensional effective-medium system.

The developed framework reveals important insights of the Purcell effect for an acoustic system. On the one hand, in a hypothetical lossless scenario ($Q_{\mathrm{loss}}^{-1} = 0$), F_{peak} increases with the decrease of Q_{leak}^{-1}, where an

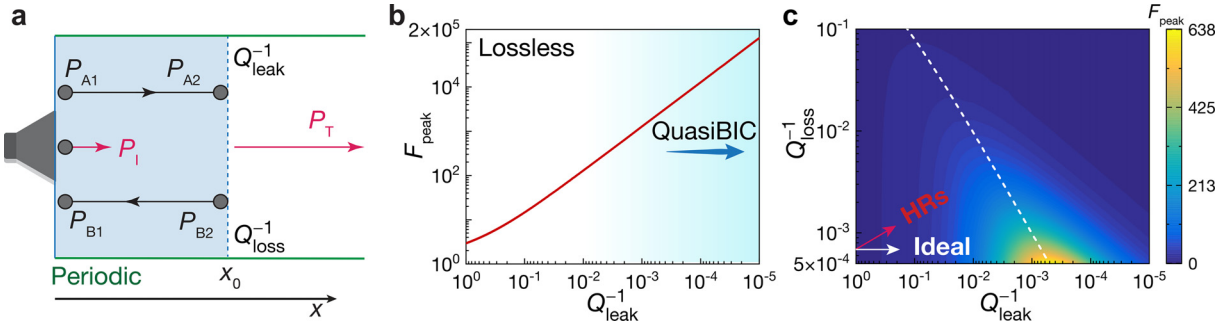

Fig. 2. Theoretical framework of the acoustic Purcell effect. (a) Wave analysis of a resonant system whose structure is theoretically treated as an effective medium and characterized by Q^{-1}_{leak} and Q^{-1}_{loss} of the dominating resonance. The sound source is at the bottom of the system. P_I represents the acoustic pressure amplitudes of waves generated by the source with a constant intensity. P_T represents the acoustic pressure amplitudes of waves emitted to the outside of the resonant system. P_{A1}, P_{A2}, P_{B1} and P_{B2} are the pressure amplitudes of decomposed waves at the bottom and front boundaries of the system. (b) Calculated F_{peak} with the variation of Q^{-1}_{leak} in the absence of Q^{-1}_{loss}. (c) Calculated F_{peak} as functions of Q^{-1}_{leak} and Q^{-1}_{loss}. The white dashed line indicates the critical emission condition.

infinitely small Q^{-1}_{leak} leads to an infinite emission enhancement (Fig. 2b). This suggests the great potential of quasiBIC systems, featured with extremely low Q^{-1}_{leak}, in stimulating the strong acoustic Purcell effect. Note that in photonic systems where the dissipative losses could often be tuned to a relatively low level (compared to acoustic systems) by carefully selecting the base material, the dissipative losses can be neglected when using a quasiBIC to realize strong emission enhancement [33]. However, in practical acoustic systems with non-trivial thermal-viscous losses, the effect of Q^{-1}_{loss} becomes crucial (see Supplementary Note 5), and optimum emission enhancement takes place under the critical emission condition (white dashed line in Fig. 2c). Evidently, to achieve a larger Purcell factor, it will be ideal that Q^{-1}_{leak} and Q^{-1}_{loss} of the system can be simultaneously modulated to lower values.

Nevertheless, the above requirements for strong Purcell effect are rather challenging in acoustic resonant systems due to the contradiction between low Q^{-1}_{leak} and low Q^{-1}_{loss}. For commonly-seen acoustic resonators such as Helmholtz resonators (HRs), a lower Q^{-1}_{leak} means less energy leaking from the openings, which subsequently demands narrower openings (necks) of the HRs. A narrower opening, in turn, leads to stronger thermal-viscous boundary layer effect [48,49] and brings about higher dissipative losses (larger Q^{-1}_{loss}) [19,46], thereby preventing us from realizing a large acoustic Purcell factor (exemplified by the red arrow in Fig. 2c). This contradiction between Q^{-1}_{leak} and Q^{-1}_{loss} of HRs is specified in detail in Supplementary Note 6.

3.3. Construction of a Friedrich–Wintgen quasiBIC-supporting system

In this study, we find that the contradiction is not inherent and can be well solved by constructing a Friedrich–Wintgen quasiBIC-supporting system (Fig. 3a), which enables the Purcell factors to theoretically reach infinite without essential contradictory restrictions. The unit cell of the periodic quasiBIC-supporting system consists of two slightly detuned resonators (cavities) with the same cross-section but different lengths (Fig. 3b). Based on the presented system, we can modulate Q^{-1}_{leak} from zero (a pure BIC) to a target value via tuning the length difference between the two cavities (l_A and l_B). In the previous study [42], a similar system was presented for extreme sound confinement of incoming sound waves from outside, while in this work we investigate the emission property of a sound source inside the quasiBIC-supporting system. The modulation of Q^{-1}_{leak} can be described by the temporal coupled-mode theory (CMT) [22,42,50–52] (see Supplementary Note 7), from which we can obtain the Hamiltonian matrix of the presented system that $-i\partial A/\partial t = HA$, $A = (\tilde{a}_A, \tilde{a}_B)^T$, with:

$$H = \begin{pmatrix} \omega_A & 0 \\ 0 & \omega_B \end{pmatrix} + i\begin{pmatrix} \gamma_A & \sqrt{\gamma_A\gamma_B} \\ \sqrt{\gamma_A\gamma_B} & \gamma_B \end{pmatrix} \tag{6}$$

where $\tilde{a}_{A(B)}$ ($= a_{A(B)}e^{i\omega t}$) represents the resonance mode of Cavity A(B), $\omega_{A(B)}$ the resonant angular frequency of Cavity A(B), $\gamma_{A(B)}$ ($= \omega_{A(B)}Q^{-1}_{leakA(B)}/2$) the corresponding radiative decay rate. Then, the two eigenvalues of H can be deduced as [53]:

$$\sigma_{\pm} = \omega_{ave} + i\gamma_{ave} \pm \sqrt{\mu^2 + (\omega_{diff} + i\gamma_{diff})^2} \tag{7}$$

where $\omega_{ave} = (\omega_A + \omega_B)/2$, $\gamma_{ave} = (\gamma_A + \gamma_B)/2$, $\omega_{diff} = (\omega_A - \omega_B)/2$ and $\gamma_{diff} = (\gamma_A - \gamma_B)/2$. $\mu = i\sqrt{\gamma_A\gamma_B}$ is the coupling coefficient of the presented system. The radiative decay rate of the system (γ_s) at the quasi-BIC can be introduced as the imaginary part of σ_-. As a proof-of-concept demonstration, we consider a structure with $w = 46$ mm, $h = 100$ mm, $b = 8$ mm and $l_A = 120$ mm. And with the tuning of l_B, it is observed from Eq. 7 that the system is in the vicinity of a BIC when the length difference of the two cavities ($\Delta l = l_B - l_A$) approaches zero (Fig. 3c).

Apart from the free tuning of Q^{-1}_{leak} shown in Fig. 3c, the system's Q^{-1}_{loss} can be modulated by changing the cross-sectional area of the cavities, where a wider cross-sectional area leads to a smaller Q^{-1}_{loss}. The system's Q^{-1}_{loss} can be calculated from the reflection property of the system [49,54–57], which is given by [58,59]:

$$Q^{-1}_{loss} = Q^{-1}_{leak}\left(\frac{1+r_0}{1-r_0}\right) \tag{8}$$

where r_0 is the reflection coefficient of the system at resonance under normal incidence. To examine intuitively how the Purcell effect of the system is governed by the dissipative losses and the quasi-BIC, we analyze the structure in Fig. 3c and assume an arbitrarily tunable Q^{-1}_{loss}. From the diagram of F_{peak} shown in Fig. 3d, it can be observed that the presented quasiBIC-supporting system has the potential to achieve optimum F_{peak} under arbitrary Q^{-1}_{loss} via changing Δl. In addition, an acoustically rigid waveguide can create a series of mirror images of the cavity unit, which is equivalent to an infinitely repeated arrangement of the building blocks. Consequently, the presented system can also achieve an infinite Q_{leak} (BIC) with one or more units in a rigid waveguide. In Supplementary Note 8, we analyze a unit cell with hard boundaries of a radiation channel, and the results only exhibit trivial differences from the results in Fig. 3c and d.

3.4. Experimental demonstration of the quasiBIC-induced acoustic Purcell effect

To verify our theoretical analysis, experiments are conducted in a steel waveguide (tube) with a length of 1460 mm and a wall thickness of 8 mm. The cross-section of the waveguide is a square with a side length of 100 mm. A unit cell of the presented structure (Fig. 3b) is fabricated by 3D-printing technology. The detailed experimental setup is presented in Supplementary Note 3. When the two cavities have a length

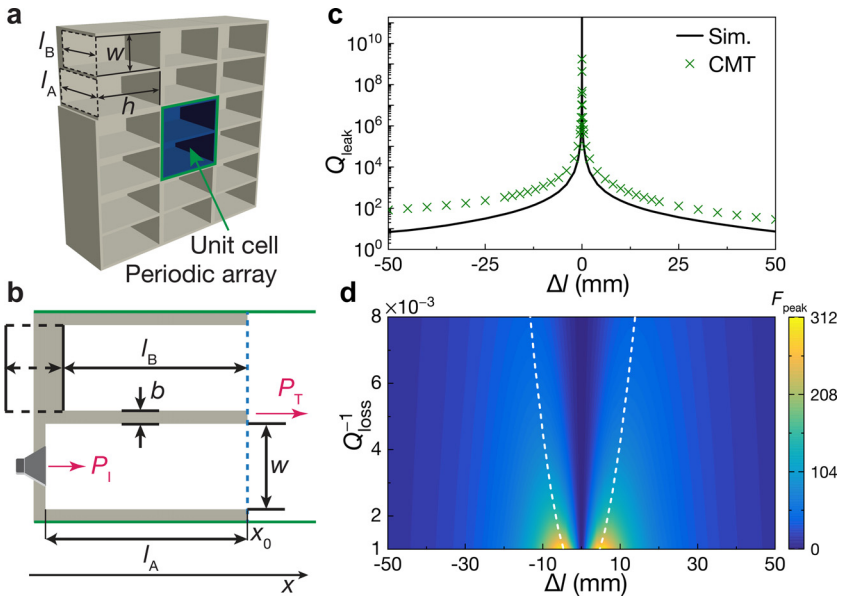

Fig. 3. Friedrich–Wintgen quasiBIC-supporting system. (a) Schematic of the system consisting of periodic unit cells. (b) The modulation of the unit cells with acoustic sources. The length of Cavity A (l_A) is fixed. The length of Cavity B (l_B) is tunable. (c) Calculated (CMT) and simulated Q_{leak} with the variation of Δl. The infinite Q_{leak} at $\Delta l = 0$ demonstrates the existence of a BIC. (d) F_{peak} with the modulation of Δl and the hypothetical free variation of Q_{loss}^{-1}. The analyzed system's geometric parameters are set to $w = 46$ mm, $h = 100$ mm, $b = 8$ mm and $l_A = 120$ mm. The white dashed line indicates the critical emission condition.

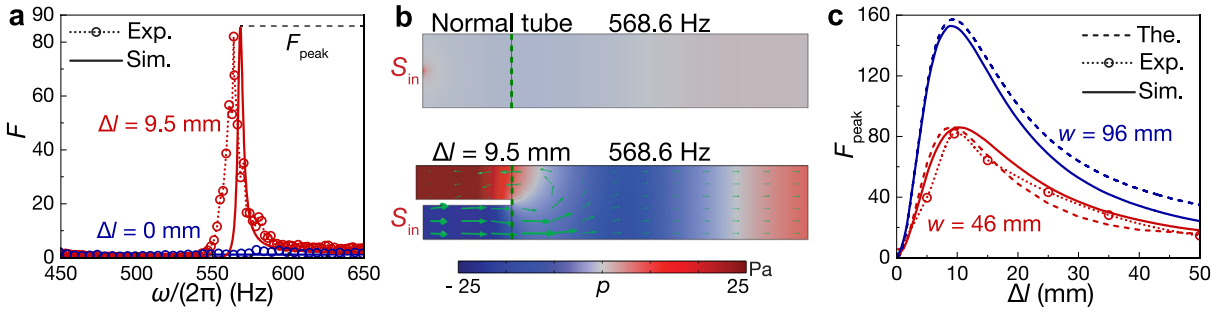

Fig. 4. Experimental demonstration of the quasiBIC-induced acoustic Purcell effect. (a) Measured and simulated results of acoustic Purcell factors (F) for $\Delta l = 9.5$ mm (red) and $\Delta l = 0$ mm (blue). (b) Simulated distributions of acoustic pressure (colors) and acoustic intensity (denoted by green arrows) of a normal tube and the presented two-state system. S_{in} denotes the sound source. (c) Calculated, Measured and simulated F_{peak} as a function of Δl. The variations of Q_{leak}^{-1} for the systems with $w = 46$ mm and $w = 96$ mm are demonstrated in Supplementary Note 10.

difference of 9.5 mm ($\Delta l = 9.5$ mm, $Q_{loss}^{-1} = 0.0037$, $Q_{leak}^{-1} = 0.0043$), large emission enhancement with a Purcell factor of 82 is experimentally achieved at 564 Hz (Fig. 4a). This result proves the existence of the strong acoustic Purcell effect induced by the quasiBIC. In addition, in the case that $\Delta l = 0$ mm, the inferior coupling condition of Q_{leak}^{-1} and Q_{loss}^{-1} suppresses the acoustic Purcell effect and the emitted waves are unable to be enhanced, which is in accordance with the results demonstrated in Fig. 3d. To further validate our results and better illustrate the acoustic Purcell effect, simulations are conducted with the commercial finite element software COMSOL Multiphysics. The simulation results agree well with the experimental results, where F_{peak} reaches 84.7 at 568.6 Hz. The frequency shift of F_{peak} between the experiment and the simulation may result from the manufacturing error of the experimental sample and other environmental factors such as temperature. Besides, the simulated acoustic pressure fields shown in Fig. 4b confirm that the quasi-BIC contributes to the confined and intensive wave energy inside the system and finally leads to the largely enhanced emitted waves [45,46]. Furthermore, the acoustic DOS of the sound field with and without the presented quasiBIC-supporting system is calculated in Supplementary Note 9, which shows a significant increase of acoustic DOS contributed by the presented system.

It is worth mentioning that the Purcell factors of the presented quasiBIC-supporting system can be consistently enhanced by further increasing the cross-sectional area of the two cavities (smaller Q_{loss}^{-1}). For instance, when the structure size is changed to $w = 96$ mm and $h = 200$ mm, the simultaneously decreased Q_{loss}^{-1} (0.002) and Q_{leak}^{-1} (0.0022) give rise to an increased F_{peak} reaching above 150 at $\Delta l = 9.5$ mm (Fig. 4c). Compared to another efficient pathway to induce the strong Purcell effect by a Mie-like resonance whose potential Purcell factor is restricted by a finite Q_{leak} [18], the quasiBIC-induced Purcell effect theoretically removes such a restriction.

4. Conclusion

We have presented the concept of the quasiBIC-induced acoustic Purcell effect, which provides a feasible and efficient pathway to achieve extreme emission enhancement. The acoustic Friedrich–Wintgen quasiBIC-supporting system overcomes the contradiction that exists in conventional acoustic structures and lifts the major upper limit of the acoustic Purcell effect. We have also developed a theoretical framework based on two fundamental factors (Q_{leak}^{-1} and Q_{loss}^{-1}), which uncovers the comprehensive physical picture of the acoustic Purcell effect and reveals the

critical emission condition. The good agreement among the experimental, simulation, and theoretical results proves the reliability of our framework. Our work opens up avenues for the study of the quasiBIC-induced acoustic Purcell effect for extreme emission enhancement, which would inspire the studies in the acoustic Purcell effect and BICs, and may find applications in high-intensity and nonlinear acoustics.

Declaration of competing interest

The authors declare that they have no conflicts of interest in this work.

Acknowledgments

This work is supported by the National Key R&D Program of China (2020YFA0211400, 2020YFA0211402) the National Natural Science Foundation of China (12074286, 11774297), the Shanghai Science and Technology Committee (21JC1405600, 20ZR1460900), and the Research Grants Council of Hong Kong SAR (AoE/P-502/20, 15205219 and C6013-18G).

Supplementary material

Supplementary material associated with this article can be found, in the online version, at doi:10.1016/j.fmre.2022.06.009.

References

[1] E.M. Purcell, H.C. Torrey, R.V. Pound, Resonance absorption by nuclear magnetic moments in a solid , Phys. Rev. 69 (1946) 37–38.
[2] C. Sauvan, J.-P. Hugonin, I. Maksymov, et al., Theory of the spontaneous optical emission of nanosize photonic and plasmon resonators , Phys. Rev. Lett. 110 (23) (2013) 237401.
[3] H. Chen, T. Liu, H. Luan, et al., Revealing the missing dimension at an exceptional point , Nat. Phys. 16 (5) (2020) 571–578.
[4] A.L. Holsteen, S. Raza, P. Fan, et al., Purcell effect for active tuning of light scattering from semiconductor optical antennas , Science 358 (6369) (2017) 1407–1410.
[5] J. Gallego, W. Alt, T. Macha, et al., Strong Purcell effect on a neutral atom trapped in an open fi ber cavity, Phys. Rev. Lett. 121 (17) (2018) 173603.
[6] S. Kato, T. Aoki, Strong coupling between a trapped single atom and an all-fiber cavity , Phys. Rev. Lett. 115 (9) (2015) 093603.
[7] E. Yablonovitch, Inhibited spontaneous emission in solid-state physics and electronics , Phys. Rev. Lett. 58 (20) (1987) 2059.
[8] J. Gérard, B. Sermage, B. Gayral, et al., Enhanced spontaneous emission by quantum boxes in a monolithic optical microcavity , Phys. Rev. Lett. 81 (5) (1998) 1110.
[9] H.N. Krishnamoorthy, Z. Jacob, E. Narimanov, et al., Topological transitions in metamaterials , Science 336 (6078) (2012) 205–209.
[10] M. Noginov, H. Li, Y.A. Barnakov, et al., Controlling spontaneous emission with metamaterials , Opt. Lett. 35 (11) (2010) 1863–1865.
[11] A.N. Poddubny, P.A. Belov, Y.S. Kivshar, Purcell effect in wire metamaterials , Phys. Rev. B 87 (3) (2013) 035136.
[12] A. Poddubny, I. Iorsh, P. Belov, et al., Hyperbolic metamaterials , Nat. Photonics 7 (12) (2013) 948–957.
[13] A. Slobozhanyuk, A. Poddubny, A. Krasnok, et al., Magnetic Purcell factor in wire metamaterials, Appl . Phys. Lett. 104 (16) (2014) 161105.
[14] K.-D. Park, T. Jiang, G. Clark, et al., Radiative control of dark excitons at room temperatur e by nano-optical antenna-tip Purcell effect, Nat. Nanotechnol. 13 (1) (2018) 59–64.
[15] A. Davoyan, H. Atwater , Quantum nonlinear light emission in metam aterials: broadband Purcell enhancement of parametric downconversion, Optica 5 (5) (2018) 608–611.
[16] M.K. Schmidt, L. Helt, C.G. Poulton, et al., Elastic Purcell effect, Phys. Rev. Lett. 121 (6) (2018) 064301.
[17] A.-W. El-Sayed, S. Hughes , Quasinormal-mode theory of elastic Purcell factors and Fano resonances of optomechanical beams, Phys. Rev. Res. 2 (4) (2020) 043290.
[18] M. Landi, J. Zhao, W.E. Prather, et al., Acoustic Purcell effect for enhanced emission, Phys. Rev. Lett. 120 (11) (2018) 114301.
[19] Y. Song, J. Du, N. Jiang, et al., Strong collimated emission enhancement by acoustic metasurfaces , Phys. Rev. Appl. 12 (5) (2019) 054012.
[20] J. Zhao, L. Zhang, Y. Wu , Enhancing monochromatic multipole emission by a subw avelength enclosure of degenerate Mie resonances, J. Acoust. Soc. Am. 142 (1) (2017) EL24–EL29.
[21] F. Liu, W. Li, M. Ke, Rigorous analytical model for multipole emission enhancement using acoustic metamaterials , Phys. Rev. Appl. 10 (5) (2018) 054031.
[22] C.W. Hsu, B. Zhen, A.D. Stone, et al., Bound states in the continuum , Nat. Rev. Mater. 1 (2016) 16048.
[23] A.F. Sadreev, Interference traps waves in an open system: bound states in the continuum , Rep. Prog. Phys. 84 (5) (2021) 055901.
[24] P. Vincent, M. Nevire , Corrugated dielectric waveguides: A numerical study of the second-order stop bands, Appl. Phys. 20 (4) (1979) 345–351.
[25] V.N. Astratov, I.S. Culshaw, R.M. Stevenson, et al., Resonant coupling of near-infrared radiation to photonic band structure waveguides , J. Lightwave Technol. 17 (11) (1999) 2050–2057 .
[26] H. Friedrich, D. Wintgen, Interfering resonances and bound states in the continuum , Phys. Rev. A 32 (6) (1985) 3231.
[27] A. Kodigala, T. Lepetit, Q. Gu, et al., Lasing action from photonic bound states in continuum , Nature 541 (2017) 196–199.
[28] H.M. Doeleman, F. Monticone, W. den Hollander, et al., Experimental observation of a polarization vortex at an optical bound state in the continuum , Nat. Photonics 12 (2018) 397.
[29] C. Huang, C. Zhang, S. Xiao, et al., Ultrafast control of vortex microlasers , Science 367 (6481) (2020) 1018–1021.
[30] Q. Song, J. Hu, S. Dai, et al., Coexistence of a new type of bound state in th e continuum and a lasing threshold mode induced by PT symmetry, Sci. Adv. 6 (34) (2020) eabc1160.
[31] N. Bernhardt, K. Koshelev, S.J. White, et al., Quasi-BIC resonant enhancement of second-harmonic generation in WS_2 monolayers, Nano Lett. 20 (7) (2020) 5309–5314.
[32] K. Koshelev, A. Bogdanov, Y. Kivshar, Meta-optics and bound states in the continuum , Sci. Bull. 64 (12) (2019) 836–842.
[33] S. Cao, Y. Jin, H. Dong, et al., Enhancing single photon emission through quasi-bound states in the continuum of monolithic hexagonal boron nitride metasurface , J. Phys. Mater. 4 (3) (2021) 035001.
[34] R. Parker , Resonance effects in wake shedding from parallel p lates: some experimental observations, J. Sound Vib. 4 (1966) 62–72.
[35] R. Parker, W.M. Griffiths, Low frequency resonance effects in wake shedding from parallel plates , J. Sound Vib. 7 (3) (1968) 371–379.
[36] R. Parker, Resonance effects in wake shedding from parallel plates: calculation of resonant frequencies , J. Sound Vib. 5 (2) (1967) 330–343.
[37] D. Evans, C. Linton, F. Ursell, Trapped mode frequencies embedded in the continuous spectrum , Q. J. Mech. Appl. Math. 46 (2) (1993) 253–274.
[38] C. Linton, M. McIver, Trapped modes in cylindrical waveguides , Q. J. Mech. Appl. Math. 51 (3) (1998) 389–412.
[39] S. Hein, W. Koch, L. Nannen , Trapped modes and Fano resonances in two-dimens ional acoustical duct-cavity systems, J. Fluid Mech. 692 (2012) 257–287.
[40] C. Linton, M. McIver, P. McIver, et al., Trapped modes for off-centre structures in guides , Wave Motion 36 (1) (2002) 67–85.
[41] L. Huang, Y. Chiang, S. Huang, et al., Sound trapping in an open resonator , Nat. Commun. 12 (2021) 4819.
[42] S. Huang, T. Liu, Z. Zhou, et al., Extreme sound confinement from quasibound states in the continuum , Phys. Rev. Appl. 14 (6) (2020) 021001.
[43] L. Cao, Y. Zhu, S. Wan, et al., Perfect absorption of flexural waves induced by bound state in the continuum , Extreme Mech. Lett. 47 (2021) 101364.
[44] L. Cao, Y. Zhu, Y. Xu, et al., Elastic bound state in the continuum with perfect mode conversion , J. Mech. Phys. Solids 154 (2021) 104502.
[45] M. Pelton, Modified spontaneous emission in nanophotonic structures , Nat. Photonics 9 (7) (2015) 427–435.
[46] P. Lodahl, S. Mahmoodian, S. Stobbe, Interfacing single photons and single quantum dots with photonic nanostructures , Rev. Mod. Phys. 87 (2) (2015) 347.
[47] T. Biwa, Y. Ueda, H. Nomura, et al., Measurement of the Q value of a n acoustic resonator, Phys. Rev. E 72 (2) (2005) 026601.
[48] M.R. Stinson, The propagation of plane sound waves in narrow and wide circular tubes, and generalization to uniform tubes of arbitrary cross-sectional shape , J. Acoust. Soc. Am. 89 (1991) 550–558.
[49] S. Huang, X. Fang, X. Wang, et al., Acoustic perfect absorbers via Helmholtz resonato rs with embedded apertures, J. Acoust. Soc. Am. 145 (2019) 254–262.
[50] S.H. Fan, W. Suh, J.D. Joannopoulos , Temporal coupled-mode theory for the Fano resonance in optical resonators, J. Opt. Soc. Am. A. 20 (2003) 569–572.
[51] W. Zhu, S. Fang, D.T. Li, et al., Simultaneous observation of a topological edge state and exceptional point in an open and non-hermitian acoustic system , Phys. Rev. Lett. 121 (2018) 124501.
[52] W. Tan, Y. Sun, Z.G. Wang, et al., Manipulating electromagnetic responses of metal wires at the deep subwavelength scale via both near- and far-field couplings , Appl. Phys. Lett. 104 (2014) 091107.
[53] M.-A. Miri, A. Alù, Exceptional points in optics and photonics , Science 363 (6422) (2019) eaar7709.
[54] S. Huang, Z. Zhou, D. Li, et al., Compact broadband acoustic sink with coherently coupled weak resonances , Sci. Bull. 65 (2020) 373–379.
[55] Y. Li, B.M. Assouar, Acoustic metasurface-based perfect absorber with deep subwavelength thickness , Appl. Phys. Lett. 108 (2016) 063502.
[56] S. Huang, X. Fang, X. Wang, et al., Acoustic perfect absorbers via spiral metasurfaces with embedded apertures , Appl. Phys. Lett. 113 (2018) 233501.
[57] C. Zhang, X. Hu , Three-dimensional single-port labyrinthine acoustic metama terial: perfect absorption with large bandwidth and tunability, Phys. Rev. Appl. 6 (2016) 064025.
[58] K.Y. Bliokh, Y.P. Bliokh, V. Freilikher, et al., Colloquium: unusual resonators: plasmonics, metamate rials, and random media, Rev. Mod. Phys. 80 (4) (2008) 1201.
[59] C. Qu, S. Ma, J. Hao, et al., Tailor the functionalities of metasurfaces based on a complete phase diagram , Phys. Rev. Lett. 115 (23) (2015) 235503.

Sibo Huang received the B.S. degree in physics from Tongji University in 2016. He received the Ph.D. degree in acoustics at Tongji University and the Ph.D. degree in mechanical engineering at the Hong Kong Polytechnic University. His current research interests include acoustic metamaterials, acoustic metasurfaces and noise control.

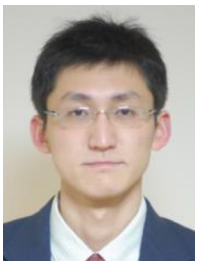

Tuo Liu (BRID: 08103.00.89658) received his Ph.D. degree in mechanical engineering from the Hong Kong Polytechnic University in 2018. He is currently a full professor at the Institute of Acoustics, Chinese Academy of Sciences. His research interests include physical acoustics, acoustic artificial structures, and non-Hermitian acoustics.

Yong Li (BRID: 05925.00.17551) received his Ph.D. degree in acoustics from Nanjing University in 2013. He is currently a full professor at Tongji University. His current research interests focus on acoustic functional materials, non-Hermitian acoustics, and advanced broadband absorbers/liners.

Jie Zhu (BRID: 05219.00.59330) received his Ph.D. degree in materials engineering from the Pennsylvania State University in 2008. He is currently a full professor at Tongji University. His research focuses on structured acoustic materials and metamaterials, and acoustic imaging technology and system.